

# Hierarchical Functionality Prioritization in Multicast ISAC: Optimal Admission Control and Discrete-Phase Beamforming

Luis F. Abanto-Leon and Setareh Maghsudi

**Abstract**—We investigate the joint admission control and discrete-phase multicast beamforming design for integrated sensing and communications (ISAC) systems, where sensing and communications functionalities have different hierarchies. Specifically, the ISAC system first allocates resources to the higher-hierarchy functionality and opportunistically uses the remaining resources to support the lower-hierarchy one. This resource allocation problem is a nonconvex mixed-integer nonlinear program (MINLP). We propose an exact mixed-integer linear program (MILP) reformulation, leading to a globally optimal solution. In addition, we implemented three baselines for comparison, which our proposed method outperforms by more than 39%.

**Index Terms**—Integrated sensing and communications, multicast, beamforming, discrete phases, admission control.

## I. INTRODUCTION

Integrated sensing and communications (ISAC) is a disruptive advancement in wireless technology in which sensing and communications share the same radio resources, e.g., infrastructure, spectrum, waveform, to enhance radio resource utilization, reduce costs, and simplify system complexity [1].

Sensing at high frequencies is appealing since the shorter wavelengths enable finer resolution [2]. These frequencies suffer severe path loss, which beamforming can alleviate. Highly versatile digital beamformers are expensive to manufacture for such high frequencies. Hence, analog beamformers lead the initial stages of ISAC systems operating at these frequencies.

Analog beamformers can be designed with continuous or discrete phases. The state-of-the-art literature features beamforming designs with both phase types, but most works focused on continuous phases, e.g., [3]–[5], while a few accounted for discrete phases, e.g., [6]. The latter are of immense practical interest, as they reduce system complexity and costs. To date, however, only suboptimal beamforming designs exist for ISAC systems that utilize discrete phases.

Another characteristic of analog beamformers is their single radio-frequency (RF) chain, which supports one signal stream, making them well-suited for multicasting scenarios, such as broadcasting live sports or concerts to several subscribed users simultaneously. Multicast beamforming has been well investigated in non-ISAC systems, e.g., [7], [8], but rarely in ISAC systems, with only a few studies addressing the topic, e.g., [9]. Yet, none of such studies accounted for constant-modulus discrete phases. Particularly, multicasting and ISAC could play a key role in live events where drones are often used for aerial filming. Thus, ISAC could enable drone tracking while supporting efficient content dissemination to users.

In non-ISAC systems, admission control is crucial in preventing resource allocation infeasibility, especially when radio resources are limited, allowing to serve only a selected subset

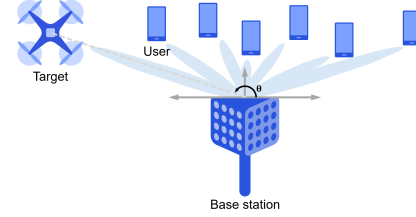


Fig. 1: Multicast ISAC system with many users and a target.

of users [8], [10], thereby enhancing resource utilization. In light of its advantages, incorporating admission control into ISAC systems holds significant promise. However, despite its potential, this aspect has been overlooked in ISAC contexts.

Moreover, angular positions of targets may not be known precisely due to factors such as motion. Thus, accounting for this aspect in the resource allocation design can help mitigate potential performance degradation in sensing, a crucial aspect explored in only a few studies, such as [11].

In ISAC systems, one functionality may be more critical than the other [12]. Particularly, this view aligns with industry’s pragmatic stance of preserving communication performance, while enabling sensing opportunistically when feasible. While tradeoff functions can balance the importance of functionalities by using weights [13], changes in parameter settings (e.g., number of users, transmit power) can skew objective function values, rendering preset weights ineffective and shifting the intended operating point. To address this, we propose establishing strict hierarchies through careful weight design. Our approach consistently prioritizes communications regardless of parameter settings, ensuring its full optimization before addressing the sensing requirements, thus leading to a strictly tiered resource allocation framework.

Motivated by the above discussion, we investigate the joint optimization of admission control and multicast beamforming with discrete phases for ISAC systems, prioritizing communications while enabling opportunistic sensing, and accounting for target angular uncertainty. This novel resource allocation problem, distinct from existing works (see Table I), is formulated as a nonconvex mixed-integer nonlinear program (MINLP), which is challenging to solve. We propose an approach to reformulate it, leading to a mixed-integer linear program (MILP) that can be solved globally optimally. Our approach employs a series of transformations to convexify the nonconvex MINLP without compromising optimality, effectively addressing the original problem’s complexity. Additionally, we implement three baselines based on well-established optimization methods used in the resource allocation literature.

**Notation:** Boldface capital letters  $\mathbf{A}$  and boldface lowercase letters  $\mathbf{a}$  denote matrices and vectors, respectively. The trans-

TABLE I: Categorization of related work.

Works	D <sub>1</sub>	D <sub>2</sub>	D <sub>3</sub>	D <sub>4</sub>	D <sub>5</sub>	D <sub>6</sub>	D <sub>7</sub>
[3]–[5]	ISAC	✗	Continuous	Unicast	✗	✗	✗
[6]	ISAC	✗	Discrete	Unicast	✗	✗	✗
[7]	Non-ISAC	✓	Discrete	Multicast	✗	✗	✗
[9]	ISAC	✗	—	Multicast	✗	✗	✗
[10]	Non-ISAC	✗	Continuous	Multicast	✓	✗	✗
[11]	ISAC	✗	Continuous	Unicast	✗	✓	✗
<b>Proposed</b>	<b>ISAC</b>	<b>✓</b>	<b>Discrete</b>	<b>Multicast</b>	<b>✓</b>	<b>✓</b>	<b>✓</b>

D<sub>1</sub>: System type  
D<sub>2</sub>: Globally optimality  
D<sub>3</sub>: Phase type  
D<sub>4</sub>: Network topology  
D<sub>5</sub>: Admission control  
D<sub>6</sub>: Angle uncertainty  
D<sub>7</sub>: Hierarchical prioritization

pose, Hermitian transpose, and trace of  $\mathbf{A}$  are denoted by  $\mathbf{A}^T$ ,  $\mathbf{A}^H$ , and  $\text{Tr}(\mathbf{A})$ , respectively. The  $l$ -th row and  $i$ -th column of  $\mathbf{A}$  are denoted by  $[\mathbf{A}]_{l,:}$  and  $[\mathbf{A}]_{:,i}$ , respectively, and the  $l$ -th element of  $\mathbf{a}$  is denoted by  $[\mathbf{a}]_l$ .  $\mathbb{C}^{I \times J}$  and  $\mathbb{N}$  denote the space of  $I \times J$  complex-valued matrices and the natural numbers, respectively. Also,  $j \triangleq \sqrt{-1}$  is the imaginary unit,  $\mathbb{E}\{\cdot\}$  denotes statistical expectation, and  $\mathcal{CN}(v, \xi^2)$  represents the complex Gaussian distribution with mean  $v$  and variance  $\xi^2$ .

## II. SYSTEM MODEL AND PROBLEM FORMULATION

We consider an ISAC system comprising a base station (BS) equipped with  $N$  transmit and  $N$  receive antennas,  $U$  single-antenna users, and one target, as shown in Fig. 1.

**Beamforming:** The BS transmits signal  $\mathbf{d} = \mathbf{w}z$ , where  $\mathbf{w} \in \mathbb{C}^{N \times 1}$  is the multicast beamforming vector and  $z \in \mathbb{C}$  is the data symbol which serves both sensing and communication purposes simultaneously, and follows a complex Gaussian distribution with zero mean and unit variance, e.g.,  $\mathbb{E}\{zz^*\} = 1$ . To account for the constant-modulus discrete phases used in the analog beamforming design, we include constraint  $C_1: [\mathbf{w}]_n \in \mathcal{S}, \forall n \in \mathcal{N}$ , where  $\mathcal{N} = \{1, \dots, N\}$  indexes the antenna elements and  $\mathcal{S} = \{\delta e^{j\phi_1}, \dots, \delta e^{j\phi_L}\}$  is the set of admissible phases. In addition,  $\delta = \sqrt{P_{\text{tx}}/N}$  is the magnitude,  $L$  is the number of phases,  $\phi_l$  is the  $l$ -th phase, and  $P_{\text{tx}}$  is the BS's transmit power. Furthermore,  $Q$  is the number of bits needed for encoding the  $L$  phases, i.e.,  $Q = \log_2(L)$ .

**Admission control:** To decide which users are served by the BS, we include constraint  $C_2: \mu_u \in \{0, 1\}, \forall u \in \mathcal{U}$ , where  $\mathcal{U} = \{1, \dots, U\}$  indexes the users. Here,  $\mu_u = 1$  indicates that user  $u$  is admitted, and  $\mu_u = 0$  otherwise.

**Communications model:** The signal received by user  $u$  is  $y_{\text{com},u} = \mathbf{h}_u^H \mathbf{d} + \eta_{\text{com},u} = \mathbf{h}_u^H \mathbf{w}z + \eta_{\text{com},u}$ , where  $\mathbf{h}_u \in \mathbb{C}^{N \times 1}$  is the channel between the BS and user  $u$ , and  $\eta_{\text{com},u} \sim \mathcal{CN}(0, \sigma_{\text{com}}^2)$  is additive white Gaussian noise (AWGN). The communication signal-to-noise ratio (SNR) at user  $u$  is

$$\text{SNR}_{\text{com},u}(\mathbf{w}) = \mathbf{w}^H \tilde{\mathbf{H}}_u \mathbf{w}, \forall u \in \mathcal{U}, \quad (1)$$

where  $\tilde{\mathbf{H}}_u = \frac{\mathbf{h}_u \mathbf{h}_u^H}{\sigma_{\text{com}}^2}$ . Let  $\Gamma_{\text{th}}$  be the minimum SNR threshold necessary for successfully decoding the multicast data. To enforce this requirement jointly with user admission, we incorporate constraint  $C_3: \mathbf{w}^H \tilde{\mathbf{H}}_u \mathbf{w} \geq \mu_u \cdot \Gamma_{\text{th}}, \forall u \in \mathcal{U}$ , i.e., the SNR threshold must be satisfied for all admitted users.

**Sensing model:** We assume the target is far from the BS, thus we model it as a single point. The BS operates as a monostatic co-located radar, i.e., the angle of departure (AoD) and angle of arrival (AoA) are the same. Hence,

the response matrix between the BS and the target is given by  $\mathbf{G}(\theta) = \alpha \mathbf{a}(\theta) \mathbf{a}^H(\theta)$ , where  $\alpha$  is the reflection coefficient,  $\theta$  is the AoD/AoA of the target, and  $\mathbf{a}(\theta) = \left[ e^{j\pi \frac{-N+1}{2} \cos(\theta)}, \dots, e^{j\pi \frac{N-1}{2} \cos(\theta)} \right]^T \in \mathbb{C}^{N \times 1}$  is the half-wavelength steering vector in the direction of  $\theta$ . The reflected signal by the target at the BS is  $y_{\text{sen}} = \mathbf{w}^H \mathbf{G}(\theta) \mathbf{d} + \eta_{\text{sen}} = \mathbf{w}^H \mathbf{G}(\theta) \mathbf{w}z + \eta_{\text{sen}}$ , where  $\eta_{\text{sen}} \sim \mathcal{CN}(0, \sigma_{\text{sen}}^2)$ . Thus, the sensing SNR, measured at the BS, is given by

$$\text{SNR}_{\text{sen}}(\mathbf{w}, \theta) = \mathbf{w}^H \tilde{\mathbf{G}}(\theta) \mathbf{w}. \quad (2)$$

where  $\tilde{\mathbf{G}}(\theta) = \frac{\mathbf{G}(\theta)}{\sigma_{\text{sen}}^2}$ . It is assumed that the transmit and receive antenna arrays are adequately spaced to prevent self-interference [14]. To account for potential uncertainty in the value of  $\theta$ , e.g., caused by the target's speed [15], we adopt the model in [11], where an angular interval  $[\theta - \Delta, \theta + \Delta]$  is considered, with  $\Delta$  representing the uncertainty in  $\theta$ . This interval is discretized into samples, resulting in set  $\Theta = \{\bar{\theta} \mid \bar{\theta} = \theta - \Delta + \frac{2\Delta}{C-1}c\}, \forall c = 0, \dots, C-1$ , where  $C$  is the number of samples taken within the interval. To ensure that the sensing SNR in all angular directions within  $\Theta$  exceeds some value  $\tau$ , we first include constraint  $C_4: \tau \geq 0$  and then add constraint  $C_5: \mathbf{w}^H \tilde{\mathbf{G}}(\theta) \mathbf{w} \geq \tau, \forall \theta \in \Theta$ .

**Objective function:** We define the tradeoff function

$$f(\boldsymbol{\mu}, \tau) \triangleq \rho_{\text{com}} \cdot f_{\text{com}}(\boldsymbol{\mu}) + \rho_{\text{sen}} \cdot f_{\text{sen}}(\tau), \quad (3)$$

which we aim to maximize. Here,  $f_{\text{com}}(\boldsymbol{\mu}) \triangleq \mathbf{1}^T \boldsymbol{\mu}$  and  $f_{\text{sen}}(\tau) \triangleq \tau$  are the objective functions related to communications and sensing, respectively. In particular,  $f_{\text{com}}(\boldsymbol{\mu})$  represents the number of admitted users, i.e., users that are served with the desired multicast data, while  $f_{\text{sen}}(\tau)$  is the lowest sensing SNR value for the angles in  $\Theta$ . In addition,  $\boldsymbol{\mu} = [\mu_1, \dots, \mu_U]^T$ , whereas  $\rho_{\text{com}}$  and  $\rho_{\text{sen}}$  are the weights that control the functionality importance.

**Problem formulation:** We formulate the joint design of admission control and discrete-phase beamforming as

$$\mathcal{P}: \underset{\mathbf{w}, \boldsymbol{\mu}, \tau}{\text{maximize}} \quad f(\boldsymbol{\mu}, \tau) \quad \text{s.t.} \quad C_1, C_2, C_3, C_4, C_5.$$

As a particular case, we consider that communications has higher hierarchy than sensing, achieved through the careful design of weights, as outlined in Lemma 1. We highlight that our framework can accommodate any arbitrary weights, even when hierarchies are not required.

**Lemma 1.** *A set of weights ensuring that communications has higher hierarchy is given by  $\rho_{\text{com}} = 1$  and  $\rho_{\text{sen}} = \frac{\sigma_{\text{sen}}^2}{2\alpha N P_{\text{tx}}}$ .*

*Proof.* To ensure that the functionalities have different hierarchies, we choose the weights such that  $\rho_{\text{com}} \cdot f_{\text{com}}(\boldsymbol{\mu})$  and  $\rho_{\text{sen}} \cdot f_{\text{sen}}(\tau)$  span nonoverlapping intervals. In particular, we let  $\rho_{\text{com}} \cdot f_{\text{com}}(\boldsymbol{\mu}) \in \mathbb{N}$  handle the integer part of  $f(\boldsymbol{\mu}, \tau)$  and let  $\rho_{\text{sen}} \cdot f_{\text{sen}}(\tau) \in [0, 1)$  handle the decimal part, thereby effectively assigning a higher hierarchy to communications. Note that  $f_{\text{com}}(\boldsymbol{\mu})$  is an integer by definition. In order for  $\rho_{\text{com}} \cdot f_{\text{com}}(\boldsymbol{\mu})$  to also be an integer, we can choose any  $\rho_{\text{com}} \in [1, \infty) \cap \mathbb{N}$ . For simplicity, we adopt  $\rho_{\text{com}} = 1$ . Besides, since  $\tau$  is smaller than or equal to  $\mathbf{w}^H \tilde{\mathbf{G}}(\theta) \mathbf{w}$ ,  $\forall \theta \in \Theta$ , as stated in  $C_5$ , we can establish an upper bound for

$\tau$  by finding an upper bound for  $\mathbf{w}^H \tilde{\mathbf{G}}(\theta) \mathbf{w}$ . Thus, we have that  $\mathbf{w}^H \tilde{\mathbf{G}}(\theta) \mathbf{w} = \frac{\alpha}{\sigma_{\text{sep}}^2} |\mathbf{w}^H \mathbf{a}(\theta)|^2$ . Applying the Cauchy-Schwarz inequality to the right-hand-side (RHS), we obtain that  $\frac{\alpha}{\sigma_{\text{sen}}^2} |\mathbf{w}^H \mathbf{a}(\theta)|^2 \leq \frac{\alpha}{\sigma_{\text{sen}}^2} \|\mathbf{a}(\theta)\|_2^2 \|\mathbf{w}\|_2^2$ . In addition, we have  $\|\mathbf{a}(\theta)\|_2^2 = N$  and  $\|\mathbf{w}\|_2^2 = P_{\text{tx}}$ , yielding  $\mathbf{w}^H \tilde{\mathbf{G}}(\theta) \mathbf{w} \leq \frac{\alpha N P_{\text{tx}}}{\sigma_{\text{sen}}^2}$  and  $f_{\text{sen}}(\tau) \leq \frac{\alpha N P_{\text{tx}}}{\sigma_{\text{sen}}^2}$ . In order for  $\rho_{\text{sen}} \cdot f_{\text{sen}}(\tau) \in [0, 1)$  to be true, we can choose any  $\rho_{\text{sen}} \in (0, \frac{\sigma_{\text{sen}}^2}{\alpha N P_{\text{tx}}})$ . For simplicity, we adopt  $\rho_{\text{sen}} = \frac{\sigma_{\text{sen}}^2}{2\alpha N P_{\text{tx}}}$ . ■

### III. PROPOSED OPTIMAL APPROACH

We introduce constraint  $C_6 : \mathbf{W} = \mathbf{w}\mathbf{w}^H$ , which contains new variable  $\mathbf{W}$  that is related to  $\mathbf{w}$ . This allows us to equivalently recast problem  $\mathcal{P}$  as problem  $\mathcal{P}'$ , shown below,

$$\begin{aligned} \mathcal{P}' : \underset{\mathbf{W}, \mathbf{w}, \boldsymbol{\mu}, \tau}{\text{maximize}} \quad & f(\boldsymbol{\mu}, \tau) \\ \text{s.t.} \quad & C_1, C_2, C_4, \\ & C_3 : \text{Tr}(\tilde{\mathbf{H}}_u \mathbf{W}) \geq \mu_u \cdot \Gamma_{\text{th}}, \forall u \in \mathcal{U}, \\ & C_5 : \text{Tr}(\tilde{\mathbf{G}}(\theta) \mathbf{W}) \geq \tau, \forall \theta \in \Theta, \\ & C_6 : \mathbf{W} = \mathbf{w}\mathbf{w}^H, \end{aligned}$$

where the trace commutative property was used in  $C_3$  and  $C_5$ . Although constraint  $C_6$  defines  $\mathbf{W}$  as rank-one, i.e., nonconvex and challenging to address, in our case  $\mathbf{W}$  arises from the product of discrete phases, encoded via binary variables. Particularly, the product of these variables can be optimally handled, as detailed in Proposition 1 to Proposition 5.

**Proposition 1.** *Constraint  $C_1$  can be equivalently rewritten as constraints  $D_1$ ,  $D_2$ , and  $D_3$ ,*

$$C_1 \Leftrightarrow \begin{cases} D_1 : [\mathbf{x}_n]_l \in \{0, 1\}, \forall n \in \mathcal{N}, l \in \mathcal{L}, \\ D_2 : \mathbf{1}^T \mathbf{x}_n = 1, \forall n \in \mathcal{N}, \\ D_3 : [\mathbf{w}]_n = \mathbf{s}^T \mathbf{x}_n, \forall n \in \mathcal{N}, \end{cases}$$

where vector  $\mathbf{s} \in \mathbb{C}^{\mathcal{L} \times 1}$  is formed by all the elements in  $\mathcal{S}$ , and  $\mathcal{L} = \{1, \dots, L\}$ .

*Proof.* Binary variables can be used to encode the phase selection for each antenna. Hence, for each antenna  $n$ , a binary vector  $\mathbf{x}_n$  is introduced, as stated in  $D_1$ . Also, only one phase per antenna must be selected, which is enforced by  $D_2$ . Finally,  $D_3$  maps  $\mathbf{x}_n$  to one of the phases in  $\mathbf{s}$ . ■

**Proposition 2.** *Constraint  $C_6$  can be equivalently rewritten as constraint  $E_1$ ,*

$$C_6 \Leftrightarrow E_1 : [\mathbf{W}]_{n,m} = [\mathbf{w}]_n [\mathbf{w}^*]_m, \forall n, m \in \mathcal{N},$$

where  $[\mathbf{W}]_{n,m}$  represents the element of  $\mathbf{W}$  in the  $n$ -th row and  $m$ -th column.

*Proof.* Given  $\mathbf{W} = \mathbf{w}\mathbf{w}^H$ , the  $n$ -th row of  $\mathbf{W}$  is  $[\mathbf{w}]_n \mathbf{w}^H$  and the  $m$ -th element of that row is  $[\mathbf{w}]_n [\mathbf{w}^*]_m$ . ■

**Proposition 3.** *Constraints  $D_3$  and  $E_1$  can be equivalently expressed as constraints  $F_1$ ,  $F_2$ , and  $F_3$ ,*

$$D_3, E_1 \Leftrightarrow \begin{cases} F_1 : [\mathbf{W}]_{n,m} = \text{Tr}(\mathbf{S} \mathbf{x}_n \mathbf{x}_m^T), \forall n \in \mathcal{N}, m \in \mathcal{M}_n, \\ F_2 : [\mathbf{W}]_{m,n} = [\mathbf{W}]_{n,m}^*, \forall n \in \mathcal{N}, m \in \mathcal{M}_n, \\ F_3 : [\mathbf{W}]_{n,n} = \delta^2, \forall n \in \mathcal{N}, \end{cases}$$

where  $\mathbf{S} = \mathbf{s}^* \mathbf{s}^T$  and  $\mathcal{M}_n = \{n+1, \dots, N\}$ .

*Proof.* Replacing  $D_3$  in  $E_1$  leads to  $[\mathbf{W}]_{n,m} = \mathbf{s}^T \mathbf{x}_n \mathbf{x}_m^T \mathbf{s}^* = \text{Tr}(\mathbf{S} \mathbf{x}_n \mathbf{x}_m^T)$ ,  $\forall n, m \in \mathcal{N}$ . Since  $E_1$  implies that  $\mathbf{W}$  is Hermitian, the elements with respect to the diagonal are conjugate symmetrical while the diagonal elements are  $\delta^2$ . Thus, instead of indexing the whole matrix  $\mathbf{W}$ , we can only index the upper triangular part as accomplished by  $F_1$ ,  $F_2$ ,  $F_3$ , thereby reducing the number of decision variables. ■

**Proposition 4.** *Constraint  $F_1$  can be equivalently expressed as constraints  $G_1$ ,  $G_2$ , and  $G_3$ ,*

$$F_1 \Leftrightarrow \begin{cases} G_1 : \mathbf{Y}_{n,m} = \mathbf{x}_n \mathbf{x}_m^T, \forall n \in \mathcal{N}, m \in \mathcal{M}_n, \\ G_2 : [\mathbf{W}]_{n,m} = \text{Tr}(\mathbf{S} \mathbf{Y}_{n,m}), \forall n \in \mathcal{N}, m \in \mathcal{M}_n, \\ G_3 : [\mathbf{Y}_{n,m}]_{l,i} \in [0, 1], \forall n \in \mathcal{N}, m \in \mathcal{M}_n, l, i \in \mathcal{L}, \end{cases}$$

*Proof.* Variable  $\mathbf{Y}_{n,m}$  is introduced to replace  $\mathbf{x}_n \mathbf{x}_m^T$ , as shown in  $G_1$ . Applying  $G_1$  to  $F_1$  leads to  $G_2$ . Finally,  $\mathbf{Y}_{n,m}$  is defined as having entries in the interval  $[0, 1]$ , as stated by  $G_3$ . Here, it is not necessary to define  $[\mathbf{Y}_{n,m}]_{l,i}$  as binary since the integrality nature is automatically enforced by  $G_1$ . ■

**Proposition 5.** *Constraint  $G_1$  can be equivalently expressed as constraints  $H_1$  and  $H_2$ ,*

$$G_1 \Leftrightarrow \begin{cases} H_1 : \mathbf{1}^T [\mathbf{Y}_{n,m}]_{:,i} = [\mathbf{x}_m]_i, \forall n \in \mathcal{N}, m \in \mathcal{M}_n, i \in \mathcal{L}, \\ H_2 : [\mathbf{Y}_{n,m}]_{l,:} \mathbf{1} = [\mathbf{x}_n]_l, \forall n \in \mathcal{N}, m \in \mathcal{M}_n, l \in \mathcal{L}, \end{cases}$$

*Proof.* Due to space constraints, the following explanation focuses solely on  $H_2$  and  $G_1$ . However, the relation between  $H_1$  and  $G_1$  is analogous, given the structural similarity between  $H_1$  and  $H_2$ . Matrix  $\mathbf{Y}_{n,m}$  is the product of binary vectors  $\mathbf{x}_n$  and  $\mathbf{x}_m^T$ , each of which has only one element 1. Hence,  $\mathbf{Y}_{n,m}$  also has one element 1 and the rest are 0. Therefore, if  $[\mathbf{x}_n]_l = 1$  and  $[\mathbf{x}_m]_i = 1$ , then  $[\mathbf{Y}_{n,m}]_{l,i} = 1$ . We use this notion to get rid of the product  $\mathbf{x}_n \mathbf{x}_m^T$ . According to  $G_1$ ,  $[\mathbf{x}_n]_l \mathbf{x}_m^T$  represents the  $l$ -th row of  $\mathbf{Y}_{n,m}$ , i.e.,  $[\mathbf{Y}_{n,m}]_{l,:} = [\mathbf{x}_n]_l \mathbf{x}_m^T$ . When  $[\mathbf{x}_n]_l = 0$ , all the elements of  $[\mathbf{Y}_{n,m}]_{l,:}$  are 0, which is equivalent to stating that the sum of all the elements of  $[\mathbf{Y}_{n,m}]_{l,:}$  is 0. When  $[\mathbf{x}_n]_l = 1$ , then  $[\mathbf{Y}_{n,m}]_{l,:} = \mathbf{x}_m^T$ . Since  $\mathbf{x}_m^T$  has one element equal to 1, then the sum of elements of  $[\mathbf{Y}_{n,m}]_{l,:}$  must be 1. ■

After applying the transformation procedures above, problem  $\mathcal{P}'$  is equivalently recast as MILP  $\mathcal{P}''$

$$\mathcal{P}'' : \underset{\mathbf{W}, \mathbf{X}, \mathbf{Y}, \boldsymbol{\mu}, \tau}{\text{maximize}} \quad f(\boldsymbol{\mu}, \tau) \quad \text{s.t.} \quad C_2, C_3, C_4, C_5, D_1, D_2, F_2, F_3, G_2, G_3, H_1, H_2.$$

Here,  $\mathbf{W}$  is not a variable but a placeholder and, therefore, it does not have to be defined as the former.

**REMARK 1.** *The worst-case computational complexity of problem  $\mathcal{P}$  is an exhaustive search (ES), which requires evaluating  $\mathcal{C}_{\text{ES}} = 2^{Q_N} \sum_{i=0}^U \binom{U}{U-i}$  candidate solutions. However, the structure of  $\mathcal{P}''$  allows us to utilize branch-and-cut (BnC) techniques, implemented in commercial solvers, which can solve  $\mathcal{P}''$  optimally at a small fraction of  $\mathcal{C}_{\text{ES}}$ . In particular, BnC operates by pruning suboptimal and infeasible candidate solutions [16], but this lies beyond the scope of this work.*

#### IV. SIMULATION RESULTS

We evaluate our proposed approach, **OPT**, for various parameter settings. We consider the Rician fading channel model, which allows line-of-sight (LoS) and non-LoS (NLoS) channel components with different contributions. Thus, the channel for user  $u$  is given by  $\mathbf{h}_u = \gamma_u \mathbf{v}_u$ , where  $\gamma_u$  accounts for large-scale fading and  $\mathbf{v}_u = \sqrt{K/(K+1)}\mathbf{v}_u^{\text{LoS}} + \sqrt{1/(K+1)}\mathbf{v}_u^{\text{NLoS}}$ ,  $\forall u \in \mathcal{U}$  is the normalized small-scale fading, with  $K$  being the Rician fading factor. The LoS component is defined as  $\mathbf{v}_u^{\text{LoS}} = \mathbf{a}(\beta_u)$ , where  $\beta_u$  is the LoS angle, and the NLoS components are defined as  $\mathbf{v}_u^{\text{NLoS}} \sim \mathcal{CN}(\mathbf{0}, \mathbf{I})$ . To compute large-scale fading, we use the UMa channel model [17], i.e.,  $\gamma_u = 28 + 22 \log_{10}(d_u) + 20 \log_{10}(f_c)$  dB, where  $f_c$  is the carrier frequency and  $d_u$  is the distance between the BS and user  $u$ . Unless specified otherwise, we consider  $f_c = 71$  GHz,  $P_{\text{tx}} = 36$  dBm,  $\sigma_{\text{com}}^2 = \sigma_{\text{sen}}^2 = -84$  dBm,  $N = 10$ ,  $U = 5$ ,  $Q = 3$ ,  $\Gamma_{\text{th}} = 30$ ,  $\Delta = 0$ ,  $C = 33$ ,  $\theta = 120$ ,  $\beta_1 = 30$ ,  $\beta_2 = 40$ ,  $\beta_3 = 50$ ,  $\beta_4 = 60$ ,  $\beta_5 = 70$ ,  $d_1 = \dots = d_5 = 40$  m,  $\mathcal{S} = \{\delta, \delta e^{j2\pi \frac{1}{2Q}}, \dots, \delta e^{j2\pi \frac{2Q-1}{2Q}}\}$ , and  $\alpha = \frac{\lambda^2 R}{64\pi^3 d^4}$ , where  $\lambda$  is the wavelength,  $R = 1$  is the radar cross-section,  $d = 20$  m is the distance between the BS and the target [18]. We used CVX and MOSEK on a laptop equipped with 16GB of RAM and an Intel Core i7@1.8GHz processor for our simulations.

**Scenario I:** We investigate the impact of the number of antennas,  $N$ , number of quantization bits,  $Q$ , and transmit power,  $P_{\text{tx}}$ , on the sensing performance,  $f_{\text{sen}}(\tau)$ . Fig. 2 shows that as  $N$  increases,  $f_{\text{sen}}(\tau)$  improves due to enhanced directivity. Similarly, higher  $P_{\text{tx}}$  allows the SNR threshold,  $\Gamma_{\text{th}}$ , to be met more easily, leaving additional power for sensing. Interestingly, increasing from  $Q = 3$  to  $Q = 5$  has minimal impact on  $f_{\text{sen}}(\tau)$ , with average differences within 5.3% between  $Q = 3$  and  $Q = 4$ , and within 6.5% between  $Q = 3$  and  $Q = 5$  when  $P_{\text{tx}} = 42$  dBm. The average runtime complexities for  $Q = 3$ ,  $Q = 4$ , and  $Q = 5$  are 0.3109, 0.9881, and 6.9847 s, respectively. Thus, in the sequel we use  $Q = 3$ . We highlight that with the current configuration, all users are served, i.e.,  $f_{\text{com}}(\mu) = 5$ . In subsequent scenarios, we show the effect of user admission on the sensing performance.

**Scenario II:** We investigate the impact of the SNR threshold,  $\Gamma_{\text{th}}$ , and target's angle uncertainty,  $\Delta$ , on communications and sensing performance. Fig. 3a shows that the number of admitted users increases as  $P_{\text{tx}}$  grows. Besides, when  $P_{\text{tx}} < 22$  dBm, no user can be served, thus all available power is allocated to sensing. At  $P_{\text{tx}} = 22$  dBm, only one user is served, while at  $P_{\text{tx}} = 28$  dBm, all users are admitted. Beyond this point, further increases in  $P_{\text{tx}}$  do not affect  $f_{\text{com}}(\mu)$  as it has reached its maximum, thus surplus power is used to enhance  $f_{\text{sen}}(\tau)$ . In Fig. 3b, the system remains in sensing-only mode over a larger  $P_{\text{tx}}$  range since  $\Gamma_{\text{th}}$  increased from 30 to 60, demanding more power per admitted user. This explains why it takes until  $P_{\text{tx}} = 26$  dBm for the system to transition into sensing and communications mode. Additionally,  $P_{\text{tx}} = 32$  dBm is needed to serve all users, compared to Fig. 3a where  $P_{\text{tx}} = 28$  dBm was sufficient. Lastly, Fig. 3c illustrates the impact of increasing angle uncertainty  $\Delta$  from 0 to 8, as compared to Fig. 3b. Despite the larger  $\Delta$ , the performance of admission control

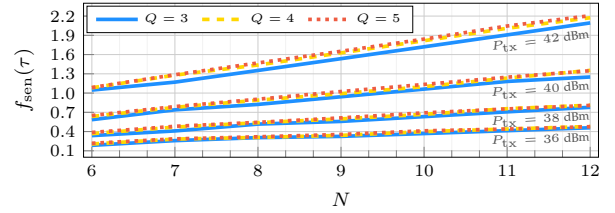
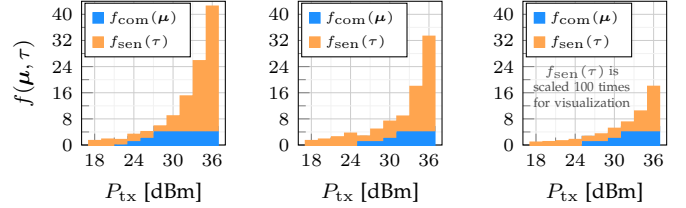


Fig. 2: Impact of the number of antennas, transmit power, and phase resolution on the sensing performance.



(a)  $\Gamma_{\text{th}} = 30$ ,  $\Delta = 0$ . (b)  $\Gamma_{\text{th}} = 60$ ,  $\Delta = 0$ . (c)  $\Gamma_{\text{th}} = 60$ ,  $\Delta = 8$ .

Fig. 3: Impact of SNR threshold and target's angle uncertainty on sensing and communications.

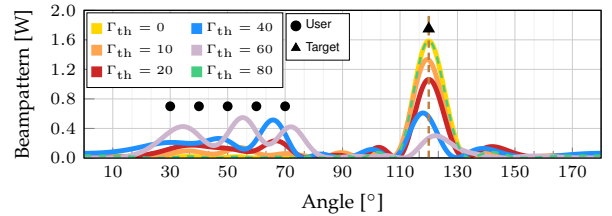


Fig. 4: Impact of SNR threshold on the beampattern.

remains unaffected, while sensing performance declines. This is because admission control takes priority, meaning that sensing is only considered after the communication functionality has been fully optimized. A larger  $\Delta$  spreads surplus power over a wider angular range, reducing power concentration in the directions of interest, degrading sensing performance. As  $f_{\text{sen}}(\tau)$  is small due to the target's reflection, we have scaled it by a factor of 100 in Fig. 3 for visualization purposes only.

**Scenario III:** We show how the beampattern adapts to meet different ISAC modes, considering  $P_{\text{tx}} = 32$  dBm. Here, we assume  $\mu_1 = \dots = \mu_5$  for admission control, allowing us to observe sharper changes in the beampattern. Fig. 4 illustrates that as  $\Gamma_{\text{th}}$  increases, the power towards the users grows, while the power illuminating the target decreases. When  $\Gamma_{\text{th}}$  becomes too high to meet for the users, the ISAC system collapses to sensing-only. That is observable with  $\Gamma_{\text{th}} = 80$ , as the produced beampattern is identical to that obtained with  $\Gamma_{\text{th}} = 0$ , demonstrating that our approach adapts to fully prioritize sensing when communications is not feasible.

**Scenario IV:** We compare **OPT** against three baselines, **BL1**, **BL2**, and **BL3**, which we implemented using well-known optimization techniques. These are briefly described below.

**Baseline 1 (BL1):** This approach is based on semidefinite relaxation (SDR), as in [3]. As the solution is not rank-one necessarily, the principal eigenvector is obtained via eigendecomposition. Afterwards, randomization and phase projection are applied to the eigenvector to meet the SNR requirements. A total of  $10^4$  randomizations are employed.

**Baseline 2 (BL2):** This approach is based on the inner

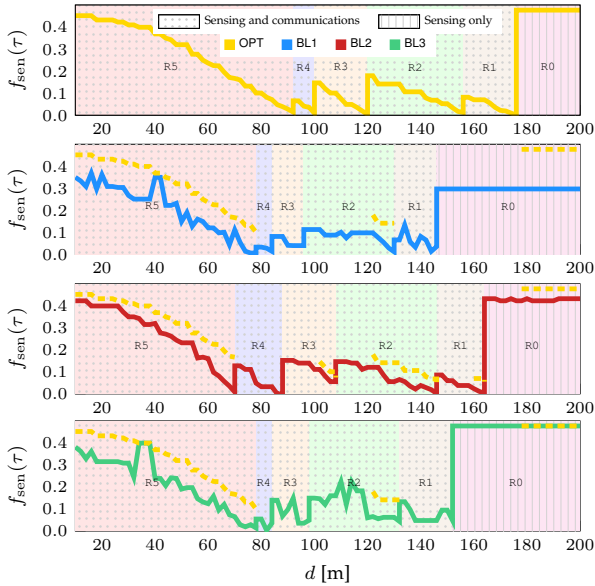


Fig. 5: Performance comparison of four different approaches.

approximation of  $C_3$  and  $C_5$ , as in [8], where a more conservative convex inequality is used to avoid dealing with the product  $\mathbf{w}\mathbf{w}^H$ . Thus, we use  $\Re(\mathbf{h}_u^H \mathbf{w}) \geq \sigma \mu_u \cdot \sqrt{\Gamma_{th}}$  instead of  $C_3: \text{Tr}(\tilde{\mathbf{H}}_u \mathbf{W}) \geq \mu_u \cdot \Gamma_{th}$ , and we do the same with  $C_5$ .

**Baseline 3 (BL3):** This approach is based on successive convex approximation (SCA), as in [5]. The obtained solution may not satisfy the set of discrete phases, thus the phases need to be projected. If the SNR constraints are not met after phase projection,  $10^4$  randomizations and projection are employed.

We demonstrate how the proposed radio resource allocation enables the ISAC system to efficiently transition between joint sensing and communication and sensing-only modes as the distance between the BS and users increases. Fig. 5 illustrates six regions RX, where X represents the number of admitted users, e.g., in R5, five users are served, while in R0, only sensing is supported. In this scenario, the distance between the BS and the users is  $d$ . As  $d$  increases, fewer users are admitted due to greater path loss, making it harder to meet the SNR threshold. Since communications take priority, larger R1–R5 regions indicate a more efficient approach. Notably, **OPT** achieves broader regions compared to the baselines, which transition between regions more rapidly, undermining communication prioritization. We plotted **OPT** where it intersected with the baselines in the same regions, and report that, within the distance range of [10, 66] m, **OPT** yields higher values, with average gains of 59%, 39%, and 47% over **BL1**, **BL2**, and **BL3**, respectively, further demonstrating its superiority. The average runtime complexities for **OPT**, **BL1**, **BL2**, and **BL3**, are 0.3867, 0.2951, 0.1917, 0.2435s, respectively.

## V. CONCLUSIONS

We investigated a novel resource allocation problem in ISAC systems, focusing on the joint design of admission control and multicast beamforming with discrete phases, while addressing different priority levels for sensing and communication. Communication was given higher priority, with its

performance measured by the number of admitted users, while sensing performance was evaluated using the sensing SNR. Our proposed approach achieves globally optimal solutions, outperforming three baseline methods and enabling broader communication operating regions.

## ACKNOWLEDGMENT

This research was supported by the German Federal Ministry of Education and Research under ‘‘Project 16KISK035’’.

## REFERENCES

- [1] F. Liu, C. Masouros, A. P. Petropulu, H. Griffiths, and L. Hanzo, ‘‘Joint radar and communication design: Applications, state-of-the-art, and the road ahead,’’ *IEEE Trans. Commun.*, vol. 68, no. 6, pp. 3834–3862, 2020.
- [2] T. Mao, J. Chen, Q. Wang, C. Han, Z. Wang, and G. K. Karagiannidis, ‘‘Waveform design for joint sensing and communications in millimeter-wave and low terahertz bands,’’ *IEEE Trans. Commun.*, vol. 70, no. 10, pp. 7023–7039, 2022.
- [3] P. Cao, ‘‘Pareto optimal analog beamforming design for integrated MIMO radar and communication,’’ pp. 1–5, 2022.
- [4] N. T. Nguyen, N. Shlezinger, Y. C. Eldar, and M. Juntti, ‘‘Multiuser MIMO wideband joint communications and sensing system with sub-carrier allocation,’’ *IEEE Trans. Signal Process.*, vol. 71, pp. 2997–3013, 2023.
- [5] W. Lyu, S. Yang, Y. Xiu, Y. Li, H. He, C. Yuen, and Z. Zhang, ‘‘CRB minimization for RIS-aided mmWave integrated sensing and communications,’’ *IEEE Internet Things J.*, vol. 11, no. 10, pp. 18 381–18 393, 2024.
- [6] L. Xu, S. Sun, Y. D. Zhang, and A. Petropulu, ‘‘Joint antenna selection and beamforming in integrated automotive radar sensing-communications with quantized double phase shifters,’’ in *Proc. of IEEE ICASSP*, 2023, pp. 1–5.
- [7] O. T. Demir and T. E. Tuncer, ‘‘Optimum discrete phase-only multicast beamforming with joint antenna and user selection in cognitive radio networks,’’ *Digit. Signal Process.*, vol. 46, pp. 81–96, 2015.
- [8] L. F. Abanto-Leon, A. Asadi, A. Garcia-Saavedra, G. H. Sim, and M. Hollick, ‘‘RadiOrchestra: Proactive management of millimeter-wave self-backhauled small cells via joint optimization of beamforming, user association, rate selection, and admission control,’’ *IEEE Trans. Wireless Commun.*, vol. 22, no. 1, pp. 153–173, 2023.
- [9] Z. Ren, Y. Peng, X. Song, Y. Fang, L. Qiu, L. Liu, D. W. K. Ng, and J. Xu, ‘‘Fundamental CRB-rate tradeoff in multi-antenna ISAC systems with information multicasting and multi-target sensing,’’ *IEEE Trans. Wireless Commun.*, vol. 23, no. 4, pp. 3870–3885, 2024.
- [10] E. Matskani, N. D. Sidiropoulos, Z.-Q. Luo, and L. Tassiulas, ‘‘Efficient batch and adaptive approximation algorithms for joint multicast beamforming and admission control,’’ *IEEE Trans. Signal Process.*, vol. 57, no. 12, pp. 4882–4894, 2009.
- [11] D. Xu, Y. Sun, D. W. K. Ng, and R. Schober, ‘‘Robust resource allocation for UAV systems with UAV jittering and user location uncertainty,’’ in *Proc. of IEEE Globecom Workshops*, 2018, pp. 1–6.
- [12] Y. Cui, F. Liu, C. Masouros, J. Xu, T. X. Han, and Y. C. Eldar, *Integrated sensing and communications: Background and applications*. Springer Nature Singapore, 2023, pp. 3–21.
- [13] A. R. Baleb and S. Maghsudi, ‘‘Piecewise-stationary multi-objective multi-armed bandit with application to joint communications and sensing,’’ *IEEE Wireless Commun. Lett.*, vol. 12, no. 5, pp. 809–813, 2023.
- [14] Z. Xiao, P. Xia, and X.-G. Xia, ‘‘Full-duplex millimeter-wave communication,’’ *IEEE Wireless Commun.*, vol. 24, no. 6, pp. 136–143, 2017.
- [15] F. Liu, Y. Cui, C. Masouros, J. Xu, T. X. Han, Y. C. Eldar, and S. Buzzi, ‘‘Integrated sensing and communications: Toward dual-functional wireless networks for 6G and beyond,’’ *IEEE Journal on Selected Areas in Communications*, vol. 40, no. 6, pp. 1728–1767, 2022.
- [16] J. Desrosiers and M. Lübbecke, ‘‘Branch-price-and-cut algorithms,’’ in *Wiley Encyclopedia of Operations Research and Management Science*, 2010.
- [17] 3GPP, ‘‘Study on channel model for frequencies from 0.5 to 100 GHz,’’ 3rd Generation Partnership Project (3GPP), Technical Report (TR) 38.901, 2020, version 16.1.0.
- [18] R. Wen, Y. Zhang, Q. Li, and Y. Tang, ‘‘Joint secure communication and radar beamforming: A secrecy-estimation rate-based design,’’ *Wirel. Commun. Mob. Comput.*, no. 1, pp. 1–17, 2022.